Mapping the Reactivity of Dicobalt Bridging Nitrides in Constrained Geometries

Ariana Z. Spentzos, Neil C. Tomson*

Roy and Diana Vagelos Laboratories, Department of Chemistry, University of Pennsylvania, 231 South 34th Street, Philadelphia, Pennsylvania, 19104, USA

ABSTRACT: Low-nuclearity nitrides of the late transition metals are rare and reactive molecular species, with little experimental precedent. The first putative examples of dicobalt bridging nitrides, $[(^{n}PDI_2)Co_2(\mu\text{-}N)(PMe_3)_2][OTf]_3$ (^{n}**[Co$_2$N]$^{3+}$**; PDI = pyridyldiimine; n = 2 or 3, representing the length of the aliphatic chain linking PDI imino groups), were reported recently and shown to undergo a range of intramolecular reaction pathways, including N–H bond formation, C–H bond insertion, and P=N bond formation at the bridging nitride. The specific mode of reactivity changed with the phase of the reaction and the size of the macrocycle used to support the transient species. The present contribution offers a computational investigation into both the geometric and electronic structures of these nitrides as well as the factors governing their reaction selectivity. The compounds ^{n}**[Co$_2$N]$^{3+}$** exhibit μ-N-based LUMOs that are consistent with subvalent, electrophilic nitrides. The specific orientations of the LUMOs induce ring-size dependent stereoelectronic effects, thereby causing the product selectivity observed experimentally. Notably, the nitrides also exhibit a degree of nucleophilicity at μ-N by way of a high energy, μ-N-based lone pair. This ambiphilic character appears to be a direct result of the constrained environment imposed by the folded-ligand geometries of ^{n}**[Co$_2$N]$^{3+}$**. When combined with the experimental findings, these data led to the conclusion that the folded-ligand isomers are the reactive species and that the constrained geometry imposed by the macrocyclic ligand plays an important role in controlling the reaction outcome.

INTRODUCTION

Surface nitrides play critical roles in a number of industrial chemical processes.[1] Most notable are the Haber-Bosch process for dinitrogen reduction[2] and the Ostwald process for ammonia oxidation,[3] both of which are used in the industrial production of fertilizers. These processes most commonly use metals from Groups 8 and 9 on the periodic table and show an activity dependence on the crystal face of the catalyst,[4-7] indicating that the placement and restructuring capacity of surface atoms impact the activity of a given crystal face. Molecular bridging nitride complexes are typically unreactive and do not capture the unique multinuclear geometries of surface nitrides (Figure 1, top and middle). It is thus of interest to evaluate the electronic structures and reactivity profiles of molecular bridging nitrides in constrained geometries.[8] Doing so is expected to provide insight into a range of heterogeneous (and enzymatic) systems that constrain the geometries of multinuclear active sites,[9, 10] while simultaneously leading to the development of new classes of molecular catalysts.

The importance of control over the spatial arrangement of metal centers in catalytic systems has recently inspired the design of multinucleating ligands designed to tune the nature and extent of M–M interactions.[11-17] We have worked with one such ligand class, $^{n}PDI_2$ (Figure 1, bottom), that uses geometric and electronic flexibility to support bimetallic complexes.[18, 19] This work has led to species that bind small molecules in geometries that are uncommon to molecular chemistry but bear some relevance to surface species.[20] Importantly, $^{n}PDI_2$ can reversibly fold and unfold, adopting a range of geometries in response to changes at the cluster core.[18, 21] This flexibility is tempered, however, by the macrocyclic structure of the ligand, which offers some constraints on the system and appears to prevent its complexes from falling into thermodynamic sinks.[20, 21] Previously, we described the use of the $^{n}PDI_2$ ligand set to support the putative formation of the first examples of dicobalt bridging nitrides (Figure 1, bottom).[22] The electronic structure and reactivity profiles of these nitrides constitute the basis of the computational study described below.

In addition to their industrial relevance, low-nuclearity cobalt nitrides are of interest due to their rarity and high reactivity. A pair of *terminal* nitrides have been proposed in the literature,[23, 24] and another terminal nitride was observed by EPR spectroscopy following photolysis at 10 K.[25] These species all appear to undergo intramolecular electrophilic reactivity, including C–H activation or other proton-coupled electron transfer (PCET) chemistry. Recently, Fortier and coworkers described the first example of an *isolable* dicobalt bridging nitride, $[Na(thf)_4][(guan)_2Co_2(\mu\text{-}N)(N_3)_2]$ (guan = (^{t}Bu$_2$CN)C(NDipp)$_2$, Dipp = 2,6-iPr$_2$-C$_6$H$_3$). This species was found to be capable of intermolecular reactivity with C–H bonds and H_2.[26] In comparison, the $^{n}PDI_2$-supported complexes appeared to form transiently before undergoing

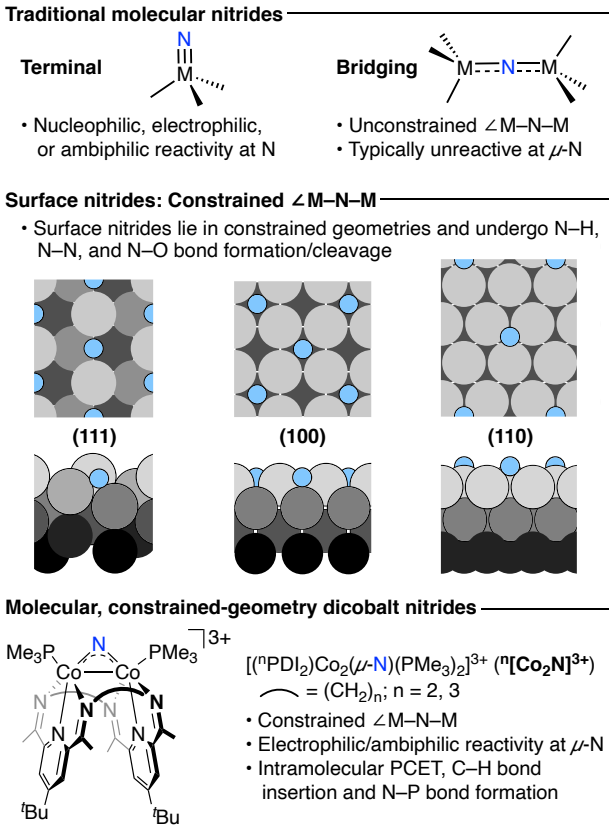

Figure 1. Top: General comparison of terminal and bridging nitrides in molecular transition metal complexes. Middle: Birds-eye (top) and side-on (bottom) views of various bcc lattice planes that form nitrides (blue) on metallic surfaces (greyscale; shade indicates the depth of the metal atom from the surface). Bottom: The constrained-geometry, dicobalt bridging nitrides that form the basis for the present DFT computation study.

a range of intramolecular reactions, including PCET to form new N–H bonds, intramolecular nitride insertion into an aliphatic C–H bond, and N–P bond coupling to a tertiary phosphine to form a bridging phosphinimide linkage. These reputed bridging nitrides notably displayed reaction selectivity based on the size of the macrocyclic ligand supporting the cluster core.

The published experimental data left a number of unanswered questions about the reactivity of these systems, but the fleeting nature of the nitrides has prevented meaningful kinetics studies. We have thus endeavored to gain insight into the reaction selectivity by performing density functional theory (DFT) calculations. The aims of this study were to examine the electronic structures of this unique class of bridging nitrides, the range of conformational isomers available to them, and the means by which the size of the macrocycle imparts reaction selectivity. The results from this study offer a view into the electrophilic reactivity of several $Co_2(\mu$-N)-containing species and highlight the impact of a constrained, multinuclear system on the properties of the bridging nitride.

Scheme 1. Isolated products from the ^{3}PDI$_2$-supported (top) and ^{2}PDI$_2$-supported (bottom) bridging nitrides.

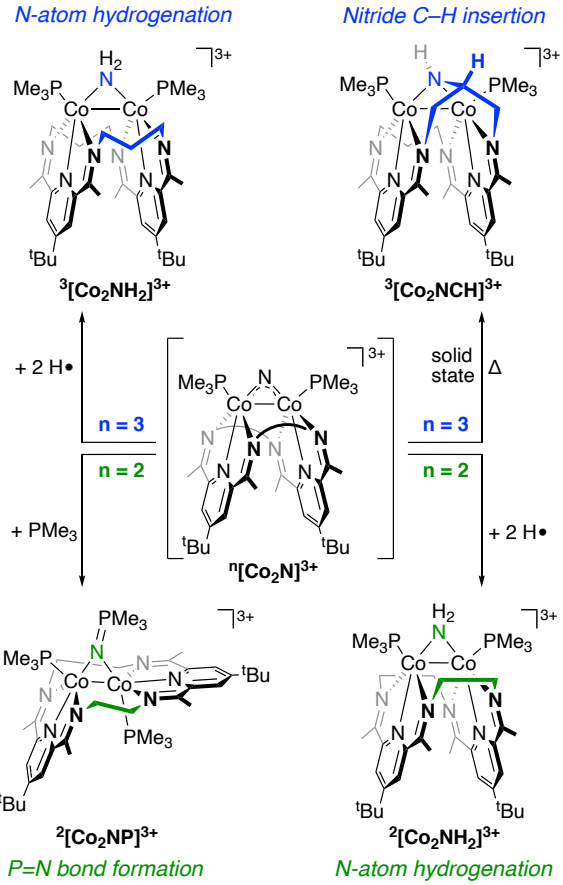

RESULTS AND DISCUSSION

Summary of key experimental results. We recently reported experimental work on the putative formation of the dicobalt bridging nitrides $[(^n$PDI$_2)$Co$_2(\mu$-N$)$(PMe$_3)_2$][OTf]$_3$ (**^{n}[Co$_2$N]$^{3+}$**, n = 2, 3; Scheme 1, center). These species were formed through spontaneous, intramolecular azide activation at the μ-N$_3$ adducts **^{n}[Co$_2$N$_3$]$^{3+}$** and were supported by a dinucleating ligand (^{n}PDI$_2$) comprised of two pyridyldiimine units linked through their imino nitrogens by n catenated methylene groups. The number of methylene groups per linker (n = 2, 3) controls the size of the macrocyclic ligand and was found to affect the reactivity of **^{n}[Co$_2$N]$^{3+}$**. The nitrides **^{n}[Co$_2$N]$^{3+}$** were not observed directly but were evidenced by a range of characteristic reaction products.

Proton-coupled electron transfer (PCET), net C–H bond insertion, and phosphine attack to form a phosphinimide ($R_3P{=}N^-$) are hallmarks of highly reactive, electrophilic nitrides, though this reactivity is rare at bridging nitrides.[26, 27] PCET by a terminal, Fe(IV) nitride led to the production of NH$_3$,[28] and in other cases, terminal, late-metal nitrides were shown to undergo various C–H activation mechanisms,[23, 29-37] including PCET from a C–H bond prior to radical rebound.[29-32] These latter examples resulted in the net insertion of the nitride into C–H bonds to form primary amido ligands. Phosphine addition has historically been used as a test for the electrophilic character of nitrides,[29] but several recent reports have highlighted that,

in addition to attack of the phosphine on an electrophilic portion of the nitride, a nitride lone pair may also donate into a P–C σ* orbital during the formation of phosphinimide ligands, suggesting that ambiphilic character of nitrides may be important to their reaction profiles.[38-40]

Depending on the reaction conditions, the size of the macrocycle, and the phase of the reaction available to ^{n}**[Co$_2$N]$^{3+}$**, the products of *i*) net hydrogenation of the nitride, *ii*) net C–H insertion of the nitride, and *iii*) P=N bond formation were isolated in reproducible yields as crystalline materials (Scheme 1). For each linker length, two products could be isolated. Solution-phase thermolysis of the isolable ^{3}**[Co$_2$N$_3$]$^{3+}$** resulted in an intractable mixture of products until PMe_3 and/or H_2 were added to the reaction mixture. In those cases, the μ-NH_2 complex ^{3}**[Co$_2$NH$_2$]$^{3+}$** was reliably isolated from the mixture, with the highest yields resulting when PMe_3 and H_2 were added at the same time. The origin of the H_2-equivalent needed to form ^{3}**[Co$_2$NH$_2$]$^{3+}$** from ^{3}**[Co$_2$N]$^{3+}$** in the absence of molecular H_2 was not identified. When performing the reaction under H_2, substituting D_2 for H_2 led to the incorporation of D on the ligand's alkyl linker, with the μ-NH_2 position remaining fully protiated. This suggested that intramolecular C–H activation yielded the μ-NH_2 moiety, then subsequent intermolecular reactivity provided the H_2-equivalent needed for reduction to form ^{3}**[Co$_2$NH$_2$]$^{3+}$**. This view was supported on isolation of the second product that appeared to have traversed through ^{3}**[Co$_2$N]$^{3+}$**. Upon thermolysis of the azide complex ^{3}**[Co$_2$N$_3$]$^{3+}$** in the solid state, the product of nitride insertion into a C–H bond of the central methylene group of the propylene linker, ^{3}**[Co$_2$NCH]$^{3+}$**, was isolated in near-quantitative yield.

Use of the smaller macrocycle, $^{2}PDI_2$, similarly generated a μ-NH_2 adduct, ^{2}**[Co$_2$NH$_2$]$^{3+}$**. This product was consistently isolated alongside a complex (^{2}**[Co$_2$NP]$^{3+}$**) containing a bridging phosphinimide ligand (μ-$NPMe_3$), a unit that was not observed to form in the $^{3}PDI_2$-supported system. While ^{2}**[Co$_2$N$_3$]$^{3+}$** was not isolable, we note that EXSY NMR spectroscopy on ^{3}**[Co$_2$N$_3$]$^{3+}$** was used to show that PMe_3 ligation to the bridging azide species is not labile. In the case of the smaller macrocycle, the yield of ^{2}**[Co$_2$NH$_2$]$^{3+}$** showed little dependence on the presence of added PMe_3, but the inability to isolate the μ-N_3 adduct of the smaller macrocycle prevented evaluation of its solid-state reactivity.

As described in the introduction, the PCET, C–H amination and phosphinimine formation reactivity observed with this system collectively support the intermediacy of the bridging nitride ^{n}**[Co$_2$N]$^{3+}$**. However, the only observable species by NMR spectroscopy were starting materials and products, and more detailed kinetic analyses were hampered by side products. Mechanisms involving direct reaction of the bridging azide with both PMe_3[41] and aliphatic C–H bonds[42-46] are also possible. We thus turned to the following computational study in order to validate the feasibility of a nitride intermediate and to identify the factors that govern the reaction pathways that emerge therefrom (see *Supporting Information* for computations on azide-mediated pathways). In order to build confidence in the DFT model, we sought to account for a wide range of experimental observables, including *i*) the need for elevated temperatures to initiate the formation of products from the azide; *ii*) the differing phosphinimide and amide product distributions as a function of the size of the macrocycle ligand; *iii*) the need for added PMe_3 in order to form ^{3}**[Co$_2$NH$_2$]$^{3+}$**; *iv*) the minimal effect of added PMe_3 on the formation of ^{2}**[Co$_2$NH$_2$]$^{3+}$**; *v*) the protiation of the bridging amide when the reaction was performed in the presence of D_2; and *vi*) the formation of the β-CH insertion product over the α-CH insertion product in ^{3}**[Co$_2$NCH]$^{3+}$**.

Azide precursors and N_2 loss to form ^{n}[Co$_2$N]$^{3+}$. All computations were performed at the B97 level of DFT with Grimme's D3 dispersion correction. Ahlrichs' def2-TZVP basis sets were used for Co, P, and N, and the def2-SV(P) basis sets were used on C and H (see Supporting Information for further details). Truncated version of the $^{n}PDI_2$ ligands, in which the ^{t}Bu groups were substituted with hydrogens, were used throughout, but to simplify the discussion, the computed complexes will be given the same abbreviations as their experimental counterparts. Similar computational methods and truncations have been validated previously for a range of closely related complexes.[18-20]

Table 1. Calculated and experimental bond metrics for bridging ^{n}[Co$_2$Cl]$^{3+}$, ^{n}[Co$_2$N$_3$]$^{3+}$, ^{n}[Co$_2$N]$^{3+}$, and *lin*-^{n}[Co$_2$N]$^{3+}$.

		^{2}[Co$_2$Cl]$^{3+}$	^{3}[Co$_2$Cl]$^{3+}$	^{2}[Co$_2$N$_3$]$^{3+}$	^{3}[Co$_2$N$_3$]$^{3+}$	^{2}[Co$_2$N]$^{3+}$	^{3}[Co$_2$N]$^{3+}$	*lin*-^{2}[Co$_2$N]$^{3+}$	lin-^{3}[Co$_2$N]$^{3+}$
Co-Co / Å	Exp	2.5560(6)	2.6334(4)		2.5819(4)				
	Calc	*2.535*	*2.612*	*2.504*	*2.557*	*2.490*	*2.439*	*3.114*	*3.310*
Co–(μ-X) / Å	Exp	2.2300(8)	2.2405(6)		1.9386(16)				
		2.2359(7)	2.2466(5)		1.9417(16)				
	Calc	*2.260*	*2.263*	*1.943*	*1.958*	*1.710*	*1.718*	*1.609*	*1.654*
		2.260	*2.265*	*1.944*	*1.959*	*1.711*	*1.720*	*1.625*	*1.662*
Co–N_{py} / Å	Exp	1.817(2)	1.8217(17)		1.8245(16)				
		1.817(2)	1.8222(17)		1.8234(16)				
	Calc	*1.809*	*1.812*	*1.812*	*1.816*	*1.908*	*1.909*	*1.852*	*1.869*
		1.809	*1.813*	*1.812*	*1.816*	*1.908*	*1.910*	*1.865*	*1.870*
∠py-py / deg	Exp	40.4	28.2		27.8				
	Calc	*33.2*	*17.3*	*36.8*	*18.6*	*79.4*	*12.1*	*35.4*	*33.3*
∠Co–X–Co / deg	Exp	69.82(2)	71.872(17)		83.43(6)				
	Calc	*68.2*	*70.5*	*80.2*	*81.5*	*93.4*	*90.4*	*148.6*	*173.4*

The bridging azide complexes ^{n}**[Co$_2$N$_3$]$^{3+}$** were found to have geometric and electronic structures similar to ^{n}**[Co$_2$Cl]$^{3+}$**, the bridging chloride complexes that both serve as synthons for ^{n}**[Co$_2$N$_3$]$^{3+}$** and were recently described in detail.[19, 22] All were determined to have S_{tot} = 0 ground states that result from a bonding interaction between two singly-occupied d_{z2} orbitals. The Co–Co and Co–X$_\mu$ distances undergo a modest contraction on substitution of N_3^- for Cl^- due to the smaller size of the 2p-element bridging atom, but the angles between the planes of the PDI ligands stay the same when comparing complexes with the same linker length (Table 1). For example, the experimental (calculated) angle between the planes of the PDI ligands in ^{3}**[Co$_2$Cl]$^{3+}$** is 28.2° (17.3°), and that angle is largely unchanged in its μ-N_3 analog ^{3}**[Co$_2$N$_3$]$^{3+}$**: 27.8° (18.6°).

A significant difference is apparent, however, when comparing complexes of this larger, propylene-linked ligand to those supported by the ethylene-linked ligand. The shorter linker leads to an increase in the angle between the PDI fragments, with measured (calculated) angles between the two PDI fragments of 40.4° (33.2°) for ^{2}**[Co$_2$Cl]$^{3+}$** and (36.8°) for ^{2}**[Co$_2$N$_3$]$^{3+}$** (experimental data are not available for ^{2}**[Co$_2$N$_3$]$^{3+}$**). As will be shown below, the constraints of the macrocyclic rings and the geometries imparted by the variable length of the alkyl linker impacts the product selectivity in this system.

The loss of N_2 from ^{2}**[Co$_2$N$_3$]$^{3+}$**/^{3}**[Co$_2$N$_3$]$^{3+}$** was calculated to proceed through energy barriers of 30.9/29.1 kcal/mol (^{n}**TS$_{NN}$**, Scheme 2) on the singlet potential energy surface to yield the bent nitrido species ^{n}**[Co$_2$N]$^{3+}$**. The transition state structures both displayed elongated Co$_2$N$_\mu$–N_2 bond lengths of 1.66 Å (compared to ~1.2 Å in the ground state azide structures) and short Co–Co distances of *ca*. 2.46 Å. The loss of phosphine prior to N_2 dissociation resulted in higher barriers for N_2 loss (+59.9/+57.1 kcal/mol; see Supporting Information). Furthermore, the loss of N_2 to form ^{n}**[Co$_2$N]$^{3+}$** was determined to be exergonic in both cases, with ΔG = -11.3 (^{2}PDI$_2$) and -5.8 (^{3}PDI$_2$) kcal/mol at 298 K. These results, coupled with the solid-state thermolytic data on ^{3}**[Co$_2$N$_3$]$^{3+}$** and the calculated reaction profiles described below, support the view that direct N_2 dissociation from ^{n}**[Co$_2$N$_3$]$^{3+}$** is a plausible pathway for forming bridging nitrides supported by a folded ligand geometry.[47] We note, however, that while the propylene-bridged ligand (^{3}PDI$_2$) remained folded following N_2 loss (∠py-py = 17.7° → 12.1°), the ^{2}PDI$_2$ ligand unfolded considerably on transforming from the azide to the nitride (∠py-py = 39.5° → 79.4°). As described below, this difference does not materially impact the valence electronic structures of the nitrides, but it does appear to tune the steric environment surrounding the cluster core.

A close examination of the Co$_2$N cores of ^{n}**[Co$_2$N]$^{3+}$** revealed short Co–Co distances at 2.45 Å, Co–N–Co angles near 90°, and Co–N$_\mu$ distances of 1.72 Å. The *ca*. 0.24 Å decreases in the Co–N$_\mu$ distances compared to those in ^{n}**[Co$_2$N$_3$]$^{3+}$** indicate the formation of multiple-bond character between the bridging nitrides and the metal centers. Accordingly, the Mayer bond orders for the Co–N$_\mu$ bonds in both complexes more than double from ^{n}**[Co$_2$N$_3$]$^{3+}$** (0.48) to ^{n}**[Co$_2$N]$^{3+}$** (1.11). The only isolated example of a dicobalt bridging nitride exhibits Co–N distances of 1.678(1) Å,[26] and the handful of known examples of terminal Co imidos lie in the same range (~1.65 Å).[48] The slight elongation of the Co–N$_\mu$ distances in ^{n}**[Co$_2$N]$^{3+}$** may result from the bent Co–N–Co geometry, which allows for the retention of multiple bond character but with diminished overlap. This explanation is consistent with the following analysis of the valence manifolds of ^{n}**[Co$_2$N]$^{3+}$**.

Scheme 2. Energy diagram showing loss of N_2 from ^{n}[Co$_2$N$_3$]$^{3+}$ to form ^{n}[Co$_2$N]$^{3+}$.

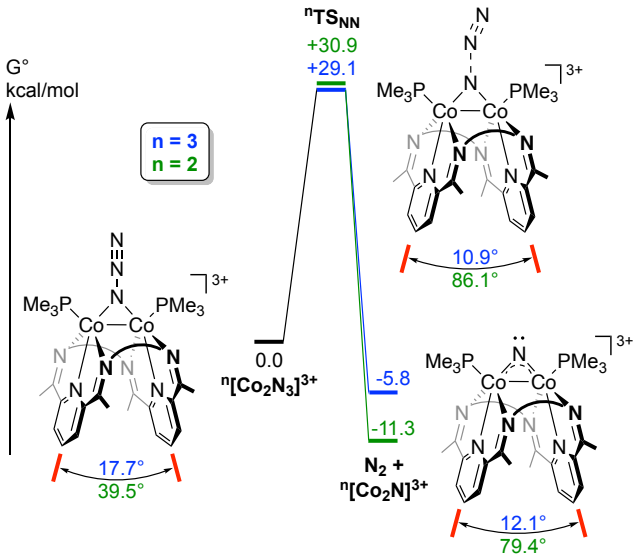

In the absence of mixing with the ancillary ligand system, a *linear* Co$_2$N fragment would exhibit degenerate, orthogonal π-(anti)bonding manifolds. For ease of comparison to the ^{n}**[Co$_2$N]$^{3+}$** system, we will focus on the presence of two electrons in the antibonding manifold, oriented as shown in Figure 2 with π* interactions in the *xy* and *yz* planes. Since these orbitals are degenerate, one would anticipate a high-spin electron configuration. Bending the Co–N–Co angle in the *yz* plane has a minimal impact on the energy of the π* interaction in the *xy* plane, but doing so removes the antibonding interaction in the *yz* plane, leading even to some bonding character at low Co–N–Co angles. In so doing, one would anticipate a preference for low-spin configurations on bending.

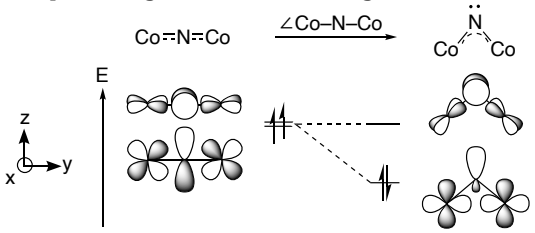

Figure 2. Qualitative Walsh diagram representing changes to the π* manifold on contraction of the Co–N–Co angle in a fragment that is isoelectronic to the cores of ^{n}**[Co$_2$N]$^{3+}$**.

Indeed, both nitrides contain a high-energy pair of electrons in the nitrido p_z and a LUMO with predominant nitrido p_x character (Figure 3). The high-lying N-based lone pair results from an orbital interaction similar to that shown in Figure 2 between N-p_z and a metal-based group orbital that may be described as [d_{yz} + d_{yz}], using the local symmetry of each metal center to define the d orbitals.

Similarly, the **^{n}[Co$_2$N]$^{3+}$** LUMOs result from an antibonding combination between μ-N-p$_x$ and a [d$_{xy}$ + d$_{xy}$] group orbital, implying the presence of an additional bonding interaction involving the p$_x$-d$_{xy}$ system. This valence structure reveals a p$_z$-based lone pair suitable for exhibiting nucleophilic character at the nitrides, while the μ-N-p$_x$ character in the molecular LUMOs offers the electrophilic character at the nitride needed for PCET reactivity, C–H insertion, and attack by a phosphine. This dual character is supported by Fukui function calculations, which identify the μ-N units as the loci of nucleophilic and electrophilic reactivity (see *Supporting Information*).

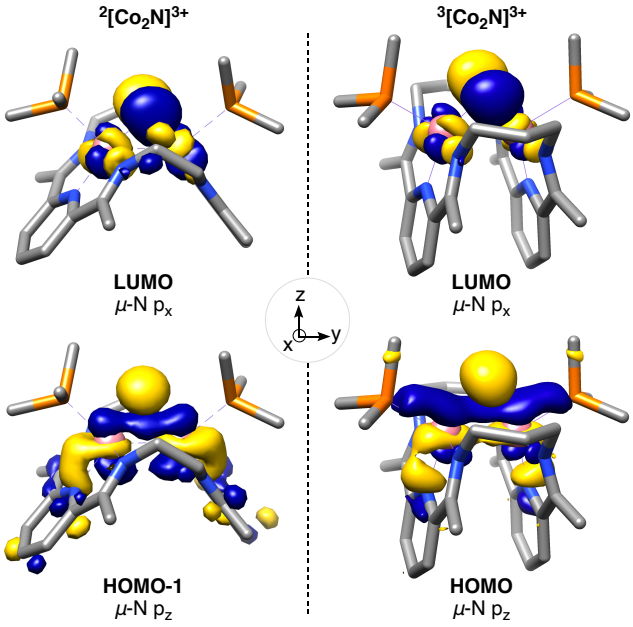

Figure 3. Frontier orbitals showing nucleophilic and electrophilic orbitals on **^{n}[Co$_2$N$_3$]$^{3+}$.**

We further attempted to determine the oxidation states of the Co and N$_\mu$ fragments in **^{n}[Co$_2$N]$^{3+}$**, but doing so is complicated by the high degree of covalency throughout the ^{n}PDI$_2$–Co–N$_\mu$ system. It is known, however, from extensive experimentally backed computational data that the bond lengths within the backbone of the ^{n}PDI$_2$ ligands in **^{n}[Co$_2$N]$^{3+}$** correspond to one electron's worth of electron density in the redox-active, π* manifold of the ligands.[19] Given this apparent –1 charge on the ^{n}PDI$_2$ ligands and the +3 charge of the cations overall, the cluster cores may be characterized as containing [Co$_2$N]$^{4+}$ units. Considering the reactivity profiles of the nitrides and the covalency in the Co–N$_\mu$ bonds that is apparent from the mixing in the valence region, the Co and N$_\mu$ centers are unlikely to express the formal [Co^{IV}–N^{3-}–Co^{III}]$^{4+}$ resonance structure. Instead, resonance structures with subvalent character at N$_\mu$, like the nitridyl structure [Co^{III}–N^{2-}–Co^{III}]$^{4+}$ and the nitrenido resonance picture [Co^{II}–N^{1-}–Co^{III}]$^{4+}$, may predominate. The latter is supported by the μ-N centered LUMOs, which reflect the vacant 2p orbital of the S = 0, 6 e$^-$ nitrenido ion. The relatively long Co–N$_{PDI}$ distances compared to the isomorphic species **^{n}[Co$_2$Cl]$^{3+}$** and **^{n}[Co$_2$NH$_2$]$^{3+}$** also support the view that the physical oxidation states of the metal centers are low (*i.e.* closer to Co^{II} than Co^{IV}), though contraction of the Co–Co distance on formation of **^{n}[Co$_2$N]$^{3+}$** complicates this analysis.

Fortier and co-workers invoked an Enemark-Feltham-type notation to collect the number of M-d and N$_\mu$-π electrons in the covalent cluster cores of Group 9 M$_2$(μ-N) species. The dinuclear Rh complex (PNN)$_2$Rh$_2$(μ-N) (PNN = [6-^{t}Bu$_2$PCH-2,2′-bipyridine]$^-$) was experimentally determined to exhibit a μ-nitridyl (N$^{\bullet 2-}$) electronic structure corresponding to {Rh$_2$N}^{17}.[49] The one-electron oxidation needed to reach the {Co$_2$N}^{16} core electron count of Fortier's dicobalt nitrides may contribute to the relative stability of [Na(thf)$_4$][(guan)$_2$Co$_2$(μ-N)(N$_3$)$_2$], owing to depopulation of the M–N$_\mu$ π* manifold. Similarly, the isolable (non-macrocyclic) PDI-supported diiridium bridging nitrides [(PDI)$_2$Ir$_2$(μ-N)]$^{+/-}$ both contain {Ir$_2$N}^{16} cores, with the redox chemistry presenting as PDI-based.[50] Notably, the Ir systems were both determined to contain μ-N$^+$ (s^{2}p^2) electronic structures, based on crystallographic, X-ray photoelectron spectroscopic, and computational data. The linear M–N–M geometries of the aforementioned Group 9 systems complicate direct comparisons to **^{n}[Co$_2$N]$^{3+}$**, but application of the Enemark-Feltham heuristic to the **^{n}[Co$_2$N]$^{3+}$** complexes results in {Co$_2$N}^{15} core electron counts, consistent with the view that **^{n}[Co$_2$N]$^{3+}$** contain highly electrophilic reaction centers.

N–H and N–P bond formations supported by the smaller, ethylene-bridged macrocycle ^{2}PDI$_2$. As described above, the presumed formation of **^{2}[Co$_2$N]$^{3+}$** was shown to lead to two isolable products, **^{2}[Co$_2$NH$_2$]$^{3+}$** and **^{2}[Co$_2$NP]$^{3+}$**. The μ-amido species, **^{2}[Co$_2$NH$_2$]$^{3+}$**, is the product of the formal addition of one equivalent of H$_2$ to **^{2}[Co$_2$N]$^{3+}$** and was proposed to result from double hydrogen atom abstraction by the transient nitride. The reaction mixture that provided **^{2}[Co$_2$NH$_2$]$^{3+}$** also yielded the phosphinimide complex, **^{2}[Co$_2$NP]$^{3+}$**, which was proposed to form via the addition of PMe$_3$ to the transient nitride, followed by a change in geometry of the macrocycle and the inclusion of an additional equivalent of PMe$_3$.

Transition states were located for both the initial N–H bond formation step (**^{2}TS$_{NH}$**) and the N–P bond formation step (**^{2}TS$_{NP}$**) (Scheme 3). **^{2}TS$_{NH}$** (ΔG‡ = +14.4/+3.1 kcal/mol vs. **^{2}[Co$_2$N]$^{3+}$**/**^{2}[Co$_2$N$_3$]$^{3+}$**) involved the abstraction of a C–H hydrogen on the ethylene linker. This abstraction process takes advantage of the twisted geometry of the macrocycle in **^{2}[Co$_2$N]$^{3+}$**, which places 2-fold symmetric hydrogen atoms within 2.2 Å of the bridging nitride. The transition state occurs when the C–H bond has elongated to 1.496 Å and the N–H bond has reached 1.177 Å. The Co–N$_\mu$ distances similarly increase to 1.804 and 1.772 Å as the bridging nitride adopts μ-imide character. The geometry of the ligand retains an obtuse angle between the pyridyl groups, consistent with the view that the to-be-abstracted hydrogen atom was in an advantageous position for PCET in the ground state ligand geometry. We were unable to locate a μ-NH intermediate with a C-based radical on the singlet surface (such a species was located on the triplet energy surface at +4.7 kcal/mol from **^{2}[Co$_2$N]$^{3+}$**). Attempts to do so led to optimization to either a radical rebound product similar to **^{3}[Co$_2$NCH]$^{3+}$** or a species with a μ-NH$_2$ unit and a dehydrogenated ethylene linker, both of which lie substantially lower in energy than **^{2}[Co$_2$N]$^{3+}$** (-29.4

Scheme 3. ***Left*: Energy diagram showing transition states to form $^{n}[Co_2NH_2]^{3+}$ and $^{n}<Co_2NP>^{3+}$. *Right*: Structures of calculated products.**

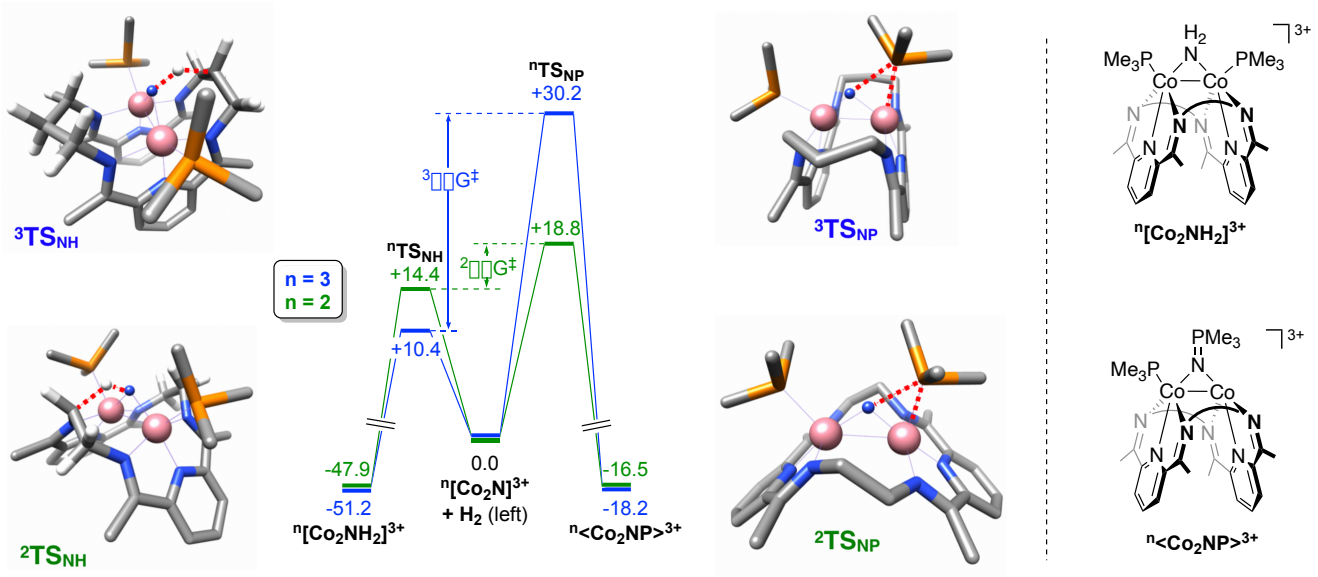

and -36.5 kcal/mol, respectively; see Supporting Information).

The transition state for the N–P bond formation step (^{2}**TS$_{NP}$**, $\Delta G^{\ddagger}$ = +18.8/+7.5 kcal/mol vs. ^{2}**[Co$_2$N]$^{3+}$**/^{2}**[Co$_2$N$_3$]$^{3+}$**) is best characterized as migration of a Co-coordinated phosphine from the metal center to the bridging nitrogen to form the μ-NPMe$_3$ complex with a single Co-coordinated phosphine, [(^{2}PDI$_2$)Co$_2$(μ-NPMe$_3$)(PMe$_3$)]$^{3+}$ (^{2}**<Co$_2$NP>$^{3+}$**, Scheme 3; the ^{n}**<Co$_2$X>** nomenclature represents a Co$_2$X core bound by ^{n}PDI$_2$ and 1 PMe$_3$ ligand to distinguish it from the ^{n}PDI$_2$ and 2 PMe$_3$ ligands of ^{n}**[Co$_2$X]**). The structure of the activated complex displays an elongated Co–P distance of 2.244 Å (the other PMe$_3$ has a Co–P distance of 2.213 Å) and a P–N$_\mu$ distance of 1.955 Å. As in the case of ^{2}**TS$_{NH}$**, the degree of ligand folding is essentially unchanged from the ground state, as expected for the modest amount of energy needed to reach the transition state. However, the orientation of the LUMO along the x-axis forces the phosphine to attack the nitrogen at an oblique angle. This causes the phosphine to interact sterically with the methylene groups of the alkyl linker on the ligand. This interaction will be discussed further below in comparison with an analogous transition state structure supported by the larger macrocycle.

The geometry of the phosphine in ^{2}**TS$_{NP}$** is also worth considering. Phosphine addition to terminal nitrides has often been used as a metric to determine the degree of electrophilicity of the nitride.[29] Electrophilic nitrides typically undergo reduction by the phosphine, while nucleophilic nitrides do not. However, two recent studies have highlighted the notion that phosphine addition to a nitride is not as simple as addition of the phosphorus-based lone-pair to a low-lying nitride-based π* orbital. Smith and co-workers have shown that a Hammett study of the reaction of various *para*-substituted phosphines with the Fe(IV) terminal nitride, PhB(MesIm)$_3$Fe(N) (MesIm = 1-(2,4,6-trimethylphenyl)inidazole-2-ylidene), revealed that the rate of the reaction increased with increasingly electron-withdrawing substitutents.[38] Theoretical investigations pointed to ambiphilic character of the nitride, involving not only a σ-symmetry interaction between the phosphine lone-pair and the nitride LUMO but also a π-symmetry interaction of the nitride HOMO and the phosphine P–C σ*. In related work, Schneider and co-workers illustrated the ability of a terminal Os nitride to undergo ambiphilic reactivity with a phosphine, involving the simultaneous donation of the phosphine lone pair into N and backbonding from the nitride into a P–C σ* orbital.[39] These interactions were evident in the transition state structure. The Os–N–P angle of 147° was significantly contracted from the linear arrangement of these atoms in the product, indicative of nucleophilic attack by the phosphine on the N p_y-based LUMO. Additionally, the presence of one obtuse N–P–C angle of 165°, along with a lengthening of the corresponding P–C distance, is consistent with backdonation into the P–C σ* orbital. A recent communication by Berry and coworkers also described direct formation of a P=N containing product formed through addition of phosphine to a coordinated azide.[41] As discussed above, however, the range of PCET and C–H insertion chemistry performed by this system lends support to a nitride intermediate.

Similar to Schneider's transition state structure, we observe geometric distortions about the migrating phosphine in ^{2}**TS$_{NP}$** that are consistent with donation of a nitride-based lone pair into a P–C σ* orbital. The phosphine adopts a see-saw geometry (max. ∠N–P–C = 145°), with a lengthened P–C distance (1.851 Å, average of 1.818 Å for the other two) for the methyl group that is *trans* to the incoming nitrogen. This view invokes both the HOMO and LUMO of ^{2}**[Co$_2$N]$^{3+}$** in N–P bond formation. The HOMO-2 of the transition state represents a bonding combination between the N-based lone pair and a P–C σ* orbital, while the HOMO results from the constructive interference of the P-based lone pair with the unoccupied, N-centered p_x that had formerly constituted the LUMO of ^{2}**[Co$_2$N]$^{3+}$** (see Supporting Information).

Importantly, the facile N–P bond formation via ^{2}**TS$_{NP}$** was found to be comparable in energy to ^{2}**TS$_{NH}$**, resulting in a $^{2}\Delta\Delta G^{\ddagger}$ = 4.4 kcal/mol in favor of ^{2}**TS$_{NH}$**. This small value for $^{2}\Delta\Delta G^{\ddagger}$ is consistent with the observation that both ^{2}**[Co$_2$NH$_2$]$^{3+}$** and ^{2}**[Co$_2$NP]$^{3+}$** are isolated from the same reaction mixture.

The experimental data for the larger macrocycle system ^{3}PDI$_2$, however, revealed crucial differences that we were interested in exploring computationally. Thermolysis of ^{3}**[Co$_2$N]$^{3+}$** was not observed to form a μ-phosphinimide product, and it required the presence of added PMe$_3$ in order to form the μ-NH$_2$ complex ^{3}**[Co$_2$NH$_2$]$^{3+}$**. This contrasts with the ^{2}PDI$_2$-supported chemistry, in which the presence of added PMe$_3$ had a negligible impact on the outcome of the reaction and was not needed in order to generate ^{2}**[Co$_2$NH$_2$]$^{3+}$**.

N–H bond formation and C–H bond insertion supported by the larger, propylene-bridged macrocycle ^{3}PDI$_2$. To generate the isolated products ^{3}**[Co$_2$NCH]$^{3+}$** and ^{3}**[Co$_2$NH$_2$]$^{3+}$** from ^{3}**[Co$_2$N]$^{3+}$**, we propose that both go through a common imide intermediate formed from PCET by the nitride (Scheme 4). With the longer alkyl linker in ^{3}**[Co$_2$N]$^{3+}$**, the possibility exists of initial PCET from two distinct positions: a CH$_2$ group α to an imino nitrogen and a CH$_2$ group β to an imino nitrogen. PCET from the β-position would require a ring flip involving movement of the central methylene group. An activation barrier for this ring flip process could not be located, but a ring-flipped ground state was identified at +2.4 kcal/mol vs. ^{3}**[Co$_2$N]$^{3+}$**. The positioning of the central methylene unit following the conformational change placed one of the hydrogen atoms at 2.142 Å from μ-N. The PCET mechanism was found to proceed through a six-membered ring transition state (^{3}**TS$_{NH}$**) and involve the direct abstraction of a hydrogen atom from a C–H bond on the alkyl linker. This step was calculated to be facile ($\Delta G^{\ddagger}$ = +10.3/+4.5 kcal/mol vs. ^{3}**[Co$_2$N]$^{3+}$**/^{3}**[Co$_2$N$_3$]$^{3+}$**) and comparable in relative energy to ^{2}**TS$_{NH}$** ($\Delta G^{\ddagger}$ = +14.4/+3.1 kcal/mol vs. ^{2}**[Co$_2$N]$^{3+}$**/^{2}**[Co$_2$N$_3$]$^{3+}$**). The activation energy for PCET from an α-CH$_2$ unit of ^{3}**[Co$_2$N]$^{3+}$** was determined to lie substantially higher in energy at +21.2 kcal/mol vs. ^{3}**[Co$_2$N]$^{3+}$**. Given this difference, and the experimental observation that the β-CH$_2$ insertion product ^{3}**[Co$_2$NCH]$^{3+}$** was isolated via solid-state thermolysis of ^{3}**[Co$_2$N$_3$]$^{3+}$**, we favor PCET from the β-position on the alkyl linker. It should be noted from the experimental side of our work that solution-phase thermolysis of ^{3}**[Co$_2$NCH]$^{3+}$** did not lead to formation of ^{3}**[Co$_2$NH$_2$]$^{3+}$**, indicating that ^{3}**[Co$_2$NCH]$^{3+}$** is not an intermediate *en route* to ^{3}**[Co$_2$NH$_2$]$^{3+}$**. Furthermore, attempts to compute transition states resulting from direct C–H insertion mechanisms were unsuccessful, supporting the view that formation of both ^{3}**[Co$_2$NH$_2$]$^{3+}$** and ^{3}**[Co$_2$NCH]$^{3+}$** proceed through a common PCET intermediate, then diverge to their products based on the reaction medium. On forming the bridging imide species ^{3}**[Co$_2$NH]$^{3+}$** (Scheme 4), abstraction of an additional hydrogen atom would generate the μ-NH$_2$ moiety, whereas radical rebound would allow for formation of ^{3}**[Co$_2$NCH]$^{3+}$**.

Scheme 4. Formation of proposed common intermediate from PCET to give ^{3}[Co$_2$NH$_2$]$^{3+}$ and ^{3}[Co$_2$NCH]$^{3+}$.

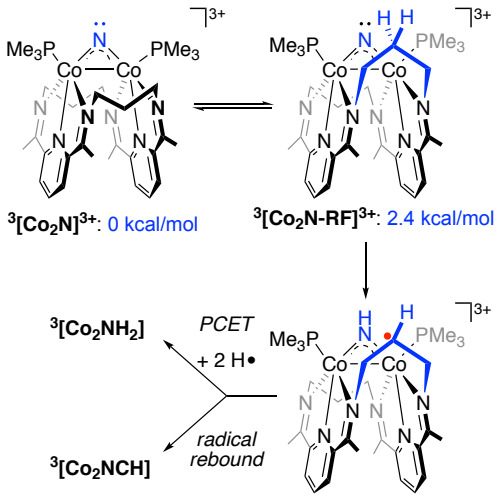

While PMe$_3$ migration to generate a phosphinimide linkage was calculated to be facile with the smaller macrocycle (^{2}**TS$_{NP}$** = +7.5/+18.8 kcal/mol vs. ^{2}**[Co$_2$N$_3$]$^{3+}$**/^{2}**[Co$_2$N]$^{3+}$**), phosphine migration with the larger macrocycle revealed a considerable energy barrier (^{3}**TS$_{NP}$** = +24.3/+30.2 kcal/mol vs. ^{3}**[Co$_2$N$_3$]$^{3+}$**/^{3}**[Co$_2$N]$^{3+}$**, Scheme 3). The resulting $^{3}\Delta\Delta G^{\ddagger}$ of 19.8 kcal/mol in favor of ^{3}**TS$_{NH}$** is much larger than the analogous value for $^{2}\Delta\Delta G^{\ddagger}$ of 4.4 kcal/mol and is consistent with the experimental observation that the larger macrocycle allows for C–H activation and *not* P–N bond formation. As mentioned above, the μ-N p_x character of the molecular LUMO of ^{n}**[Co$_2$N]$^{3+}$** (Figure 3) causes the migrating, nucleophilic phosphine to tilt out-of-plane, resulting in steric interactions between the phosphine methyl groups and the bridging methylene units. The flatter ^{n}PDI$_2$ ring in ^{2}**TS$_{NP}$** (∠py-py = 75.9°) compared to ^{3}**TS$_{NP}$** (16.4°) creates more space for phosphine migration, thereby contributing to the lower activation energy to the formation of ^{2}**<Co$_2$NP>$^{3+}$**. This can be seen in the space-filling model for ^{2}**TS$_{NP}$** and ^{3}**TS$_{NP}$** (Figure 4), where the methyl groups on the migrating phosphine are significantly more impinged by the propylene linker compared to the ethylene linker.

While these stereoelectronic effects explain the difference in P=N bond formation accessibility between the two nitrides, an unexplained experimental phosphine dependence to form ^{3}**[Co$_2$NH$_2$]$^{3+}$** also piqued our interest. The ^{3}PDI$_2$-based thermolysis of ^{3}**[Co$_2$N$_3$]$^{3+}$** to form ^{3}**[Co$_2$NH$_2$]$^{3+}$** was found to be dependent on the presence of added PMe$_3$, suggesting that PMe$_3$ dissociation was both thermally accessible and product-determining under the reaction conditions. The NMR spectroscopic technique EXSY (exchange spectroscopy) was used to determine that PMe$_3$ coordination at the azide complex ^{3}**[Co$_2$N$_3$]$^{3+}$** was inert with respect to exchange,[22] which would presumably proceed through a dissociative mechanism given the saturated coordination spheres of the Co ions. In accordance with this view, the monophosphine complex [(^{3}PDI$_2$)Co(μ-N$_3$)(PMe$_3$)]$^{3+}$ (^{3}**<Co$_2$N$_3$>$^{3+}$**) was calculated to lie 34.9 kcal/mol higher in energy than ^{3}**[Co$_2$N$_3$]$^{3+}$**. An

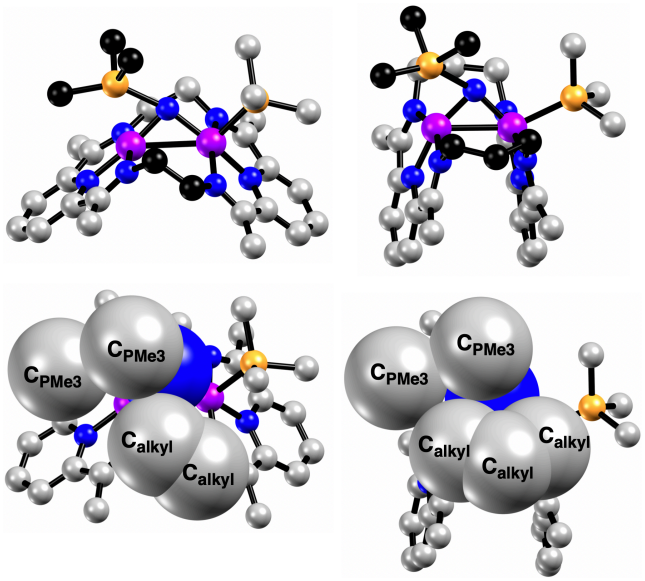

Figure 4. *Top*: Ball and stick model of ^{n}**TS$_{NP}$** with both migrating phosphine carbons and sterically interacting alkyl chains shown in black. *Bottom*: Partial space filling model of ^{2}**TS$_{NP}$** and ^{3}**TS$_{NP}$**. Migrating phosphine carbons, nitride, and alkyl linkers shown with space-filling model.

activation barrier for PMe_3 dissociation could not be located, which was not unexpected given the minimal geometric change between ^{3}**[Co$_2$N$_3$]$^{3+}$** and ^{3}**<Co$_2$N$_3$>$^{3+}$** (see Supporting Information). By comparison, phosphine loss from the bridging nitride ^{3}**[Co$_2$N]$^{3+}$** to form [(^{3}PDI$_2$)Co(μ-N)(PMe_3)]$^{3+}$ (^{3}**<Co$_2$N>$^{3+}$**) is more energetically accessible (+22.8 kcal/mol, Scheme 5). This agrees with the view that phosphine dissociation from the μ-nitride intermediate ^{3}**[Co$_2$N]$^{3+}$** may be operative in determining the reaction outcome. We note that the smaller macrocycle exhibits the same trends in phosphine dissociation energies as those outlined above. Phosphine loss is thermodynamically disfavored in all cases, but PMe_3 loss from the azide complex ^{2}**[Co$_2$N$_3$]$^{3+}$** to form ^{2}**<Co$_2$N$_3$>$^{3+}$** (+34.9 kcal/mol) is more disfavorable than PMe_3 loss from the nitride ^{2}**[Co$_2$N]$^{3+}$** to form ^{2}**<Co$_2$N>$^{3+}$** (+10.2/+21.6 kcal/mol vs. ^{2}**[Co$_2$N$_3$]$^{3+}$**/^{2}**[Co$_2$N]$^{3+}$**). Still, an important difference between the two μ-N systems was identified on investigation of their energy landscapes.

Given our previous observation that the folded and unfolded forms of the ^{n}PDI$_2$ ligand can interconvert, we reasoned that phosphine dissociation from ^{n}**[Co$_2$N]$^{3+}$** would provide the open coordination site needed to allow ligand unfolding to occur. We recently reported an isolable diiron bridging nitride that is isoelectronic to ^{3}**[Co$_2$N]$^{3+}$**.[51] The iron congener exhibits a linear μ-N linkage (Fe–N–Fe = 177.1(2)°) supported by an unfolded ligand geometry, with phosphine ligands lying on opposite sides of the macrocycle. Considering this result and the more labile coordination environments of the bridging nitrides than the bridging azides, we examined the energies of various isomers of ^{n}**<Co$_2$N>$^{3+}$** and ^{n}**[Co$_2$N]$^{3+}$** in order to survey the energetic landscape available to each (Scheme 5).

Scheme 5. Energy diagram for the interconversion of folded and unfolded geometries of ^{n}[Co$_2$N]$^{3+}$.

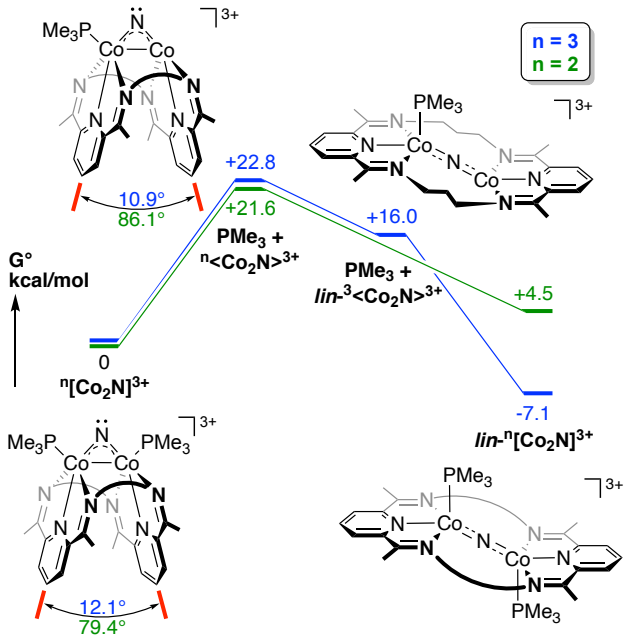

The larger pocket available from the ^{3}PDI$_2$ ligand allowed for the formation of linear μ-nitrido isomers of both the monophosphine (***lin*-^{3}<Co$_2$N>$^{3+}$**, Co–N–Co = 168.8°) and diphosphine (***lin*-^{3}[Co$_2$N]$^{3+}$**, Co–N–Co = 173.4°) complexes. Both were found to be *ca.* 7 kcal/mol more stable than their folded μ-nitrido counterparts, meaning ***lin*-^{3}[Co$_2$N]$^{3+}$** likely represents the global minimum for a Co$_2$N core bound by the larger macrocycle, ^{3}PDI$_2$, in the presence of two equivalents of PMe_3. This contrasts with the energy landscape for the smaller macrocyclic ring structure in ^{2}**[Co$_2$N]$^{3+}$**, for which the constrained pocket between the metal centers disfavors the formation of a linear nitride. A local minimum with a more obtuse Co–N–Co angle was located (***lin*-^{2}[Co$_2$N]$^{3+}$**, Co–N–Co = 148.6°) but found to lie 4.5 kcal/mol *higher* in energy than ^{2}**[Co$_2$N]$^{3+}$**.[52] Also, no energy minimum was located for a monophosphine species, ***lin*-^{2}<Co$_2$N>$^{3+}$**. This was supported by a relaxed coordinate scan (see Supporting Information) that started at the geometry of ^{2}**<Co$_2$N>$^{3+}$** (d_{CoCo} = 2.49 Å) and increased the Co–Co distance at regular intervals up to 3.1 Å (the Co–Co distance in ***lin*-^{2}[Co$_2$N]$^{3+}$**). Doing so simply resulted in a monotonic increase in the energy of the system, indicating that the *folded* diphosphine isomer, ^{2}**[Co$_2$N]$^{3+}$**, is the global minimum when a Co$_2$N core is bound by the smaller macrocycle.

Together, these data suggest that the function of added PMe_3 when forming ^{3}**[Co$_2$NH$_2$]$^{3+}$** from ^{3}**[Co$_2$N]$^{3+}$** is to prevent isomerization of the bent Co–N–Co core of ^{3}**[Co$_2$N]$^{3+}$** to a thermodynamically preferred isomer that contains a linear Co–N–Co core, ***lin*-^{3}[Co$_2$N]$^{3+}$**. The presence of additional equivalents of PMe_3 does not exhibit a similar effect on the chemistry of the smaller macrocycle since the linear isomer is thermodynamically disfavored with respect to the bent isomer. The combination of the experimental data with these computational results indicates that the bent nitrides are the species that lead to the formation of ^{n}**[Co$_2$NH$_2$]$^{3+}$**, ^{3}**[Co$_2$NCH]$^{3+}$** , and ^{2}**[Co$_2$NP]$^{3+}$**.

SUMMARY AND CONCLUSIONS

In summary, we have used DFT computations to investigate the electronic structures of a pair of rare and reactive dicobalt bridging nitrides. The complexes most notably undergo facile intramolecular PCET involving an unactivated, aliphatic C–H bond, but these systems are also of interest given the impact of geometric constraints – including the size of the macrocycle and the phase of the reaction – on their intramolecular reactivity profiles.

As proposed in the original experimental work, the formation of the bridging nitrides from bridging azide species results in μ-N groups with bent Co–N–Co moieties. The present computational work revealed the ambiphilic character of these bridging nitrides, with sp^2-hybridized, high-lying lone pairs and LUMOs largely composed of a perpendicular N-p_x, providing sites for electrophilic reactivity at the nitrides. This orbital arrangement suggests significant subvalent character at μ-N that comports with the electrophilic reactivity profiles of ^{n}**[Co$_2$N]$^{3+}$**. The LUMOs were found to be particularly important for the PCET chemistry involving C–H activation of the aliphatic linkers. The three bridging amide products, ^{n}**[Co$_2$NH$_2$]$^{3+}$** and ^{3}**[Co$_2$NCH]$^{3+}$**, were all found to form through a bridging μ-NH intermediate that resulted from facile PCET from the alkyl chain to μ-N. Subsequent radical rebound or further PCET yielded ^{3}**[Co$_2$NCH]$^{3+}$** or ^{2}**[Co$_2$NH$_2$]^{3}**, respectively.

The ambiphilic character of the nitrides was particularly important to the formation of a phosphinimide linkage supported by the smaller macrocycle. The N-p_z-based lone pair was found to act as a nucleophile, attacking the P–C σ* system, while the N-p_x character of the LUMOs forced the migrating phosphine to attack at an oblique angle, causing steric interactions with the linkers. The $\Delta\Delta G^{‡}$ for the conversion between ^{2}**[Co$_2$N]$^{3+}$** and its two *N*-functionalized products was calculated to be quite small ($^{2}\Delta\Delta G^{‡}$ = 4.4 kcal/mol), consistent with the isolation of both species from the same reaction mixture. In contrast, the barrier for forming a phosphinimide linkage from ^{3}**[Co$_2$N]$^{3+}$** was much greater than the barrier to N–H bond formation ($^{3}\Delta\Delta G^{‡}$ = 19.8 kcal/mol). The high barrier for P=N bond formation from ^{3}**[Co$_2$N]$^{3+}$** was thus attributed to the greater steric interactions between the migrating phosphine and the folded propylene chain compared to its ethylene-bridged congener.

This reactivity appears to depend, however, on the specific conformation of the nitride. A survey of the various isomers available to ^{n}**[Co$_2$N]$^{3+}$** revealed a "linear" isomer for each, ***lin***-^{n}**[Co$_2$N]$^{3+}$**. In the case of ^{2}**[Co$_2$N]$^{3+}$**, the linear isomer was found to lie thermodynamically uphill, likely due to the constraints of the macrocycle preventing a linear Co–N$_\mu$–Co arrangement (148.6°). However, the unfolded isomer for ^{3}**[Co$_2$N]$^{3+}$**, ***lin***-^{3}**[Co$_2$N]$^{3+}$**, was found to be more thermodynamically stable, and it notably allowed for a nearly linear Co–N$_\mu$–Co geometry (173.4°). This suggests that the reactivity observed experimentally occurs from the species with the folded ligand geometry. In the case of transforming ^{3}**[Co$_2$N]$^{3+}$** into ^{3}**[Co$_2$NH$_2$]$^{3+}$**, it is thus proposed that added phosphine in the reaction mixture is needed to enforce a folded ligand geometry.

This system represents a rare example of molecular cobalt nitrides, and the wide array of intramolecular reaction products found from these transient species provided ample opportunity to probe the (stereo)electronic effects brought by the unique ^{n}PDI$_2$ macrocycle. Altogether, this work highlights the potent reactivity available to bridging nitrides when they are placed in suitable coordination environments and maps a course forward for accessing challenging, intermolecular small molecule activation chemistry with multinuclear complexes.

ASSOCIATED CONTENT

Supporting Information

The Supporting Information is available free of charge on the ACS Publications website.

Supplementary computational details (PDF)

AUTHOR INFORMATION

Corresponding Author

* Email address: tomson@upenn.edu

ACKNOWLEDGMENT

We thank the National Science Foundation (CHE-1945265), the donors of the Petroleum Research Fund, administered by the American Chemical Society (57346-DNI3), and the University of Pennsylvania for financial support.

REFERENCES

1. Hargreaves, J. S. J., Heterogeneous catalysis with metal nitrides. *Coord. Chem. Rev.* **2013,** *257* (13), 2015-2031.
2. In *Catalytic Ammonia Synthesis: Fundamentals and Practice*, Jennings, J. R., Ed. Springer US: Boston, MA, 1991; pp 1-18.
3. Nitric Acid, Nitrous Acid, and Nitrogen Oxides. In *Ullmann's Encyclopedia of Industrial Chemistry*.
4. Ertl, G., Primary steps in catalytic synthesis of ammonia. *J. Vac. Sci. Technol. A* **1983,** *1* (2), 1247-1253.
5. Somorjai, G. A.; Materer, N., Surface structures in ammonia synthesis. *Top. Catal.* **1994,** *1* (3), 215-231.
6. Huo, C.-F.; Wu, B.-S.; Gao, P.; Yang, Y.; Li, Y.-W.; Jiao, H., The Mechanism of Potassium Promoter: Enhancing the Stability of Active Surfaces. *Angew. Chem. Int. Ed.* **2011,** *50* (32), 7403-7406.
7. Sadykov, V. A.; Isupova, L. A.; Zolotarskii, I. A.; Bobrova, L. N.; Noskov, A. S.; Parmon, V. N.; Brushtein, E. A.; Telyatnikova, T. V.; Chernyshev, V. I.; Lunin, V. V., Oxide catalysts for ammonia oxidation in nitric acid production: properties and perspectives. *Appl. Catal., A* **2000,** *204* (1), 59-87.
8. Tachikawa, M.; Stein, J.; Muetterties, E. L.; Teller, R. G.; Beno, M. A.; Gebert, E.; Williams, J. M., Metal clusters with exposed and low-coordinate nitride nitrogen atoms. *J. Am. Chem. Soc.* **1980,** *102* (21), 6648-6649.
9. Muetterties, E. L.; Rhodin, T. N.; Band, E.; Brucker, C. F.; Pretzer, W. R., Clusters and surfaces. *Chem. Rev.* **1979,** *79* (2), 91-137.
10. Ghosh, A. C.; Duboc, C.; Gennari, M., Synergy between metals for small molecule activation: Enzymes and bio-inspired complexes. *Coord. Chem. Rev.* **2021,** *428*, 213606.
11. Powers, T. M.; Betley, T. A., Testing the Polynuclear Hypothesis: Multielectron Reduction of Small Molecules by Triiron Reaction Sites. *J. Am. Chem. Soc.* **2013,** *135* (33), 12289-12296.
12. Shoshani, M. M.; Johnson, S. A., Cooperative carbon-atom abstraction from alkenes in the core of a pentanuclear nickel cluster. *Nat. Chem.* **2017,** *9* (12), 1282-1285.
13. Kanady, J. S.; Tsui, E. Y.; Day, M. W.; Agapie, T., A Synthetic Model of the Mn$_3$Ca Subsite of the Oxygen-Evolving Complex in Photosystem II. *Science* **2011,** *333* (6043), 733-736.
14. Wu, B.; Wilding, M. J. T.; Kuppuswamy, S.; Bezpalko, M. W.; Foxman, B. M.; Thomas, C. M., Exploring Trends in Metal–Metal Bonding, Spectroscopic Properties, and Conformational Flexibility in a Series of Heterobimetallic Ti/M and V/M Complexes (M = Fe, Co, Ni, and Cu). *Inorg. Chem.* **2016,** *55* (23), 12137-12148.

15. Ferreira, R. B.; Murray, L. J., Cyclophanes as Platforms for Reactive Multimetallic Complexes. *Acc. Chem. Res.* **2019,** *52* (2), 447-455.
16. Chatterjee, B.; Chang, W.-C.; Jena, S.; Werlé, C., Implementation of Cooperative Designs in Polarized Transition Metal Systems—Significance for Bond Activation and Catalysis. *ACS Catal.* **2020,** *10* (23), 14024-14055.
17. Cammarota, R. C.; Clouston, L. J.; Lu, C. C., Leveraging molecular metal–support interactions for H_2 and N_2 activation. *Coord. Chem. Rev.* **2017,** *334*, 100-111.
18. Zhang, S.; Wang, Q.; Thierer, L. M.; Weberg, A. B.; Gau, M. R.; Carroll, P. J.; Tomson, N. C., Tuning Metal–Metal Interactions through Reversible Ligand Folding in a Series of Dinuclear Iron Complexes. *Inorg. Chem.* **2019,** *58* (18), 12234-12244.
19. Wang, Q.; Zhang, S.; Cui, P.; Weberg, A. B.; Thierer, L. M.; Manor, B. C.; Gau, M. R.; Carroll, P. J.; Tomson, N. C., Interdependent Metal–Metal Bonding and Ligand Redox-Activity in a Series of Dinuclear Macrocyclic Complexes of Iron, Cobalt, and Nickel. *Inorg. Chem.* **2020,** *59* (7), 4200-4214.
20. Liu, T.; Gau, M. R.; Tomson, N. C., Mimicking the Constrained Geometry of a Nitrogen-Fixation Intermediate. *J. Am. Chem. Soc.* **2020,** *142* (18), 8142-8146.
21. Spentzos, A. Z.; Gau, M. R.; Carroll, P. J.; Tomson, N. C., Unusual cyanide and methyl binding modes at a dicobalt macrocycle following acetonitrile C–C bond activation. *Chem. Commun.* **2020,** *56* (67), 9675-9678.
22. Cui, P.; Wang, Q.; McCollom, S. P.; Manor, B. C.; Carroll, P. J.; Tomson, N. C., Ring-Size-Modulated Reactivity of Putative Dicobalt-Bridging Nitrides: C–H Activation versus Phosphinimide Formation. *Angew. Chem. Int. Ed.* **2017,** *56* (50), 15979-15983.
23. Hojilla Atienza, C. C.; Bowman, A. C.; Lobkovsky, E.; Chirik, P. J., Photolysis and Thermolysis of Bis(imino)pyridine Cobalt Azides: C–H Activation from Putative Cobalt Nitrido Complexes. *J. Am. Chem. Soc.* **2010,** *132* (46), 16343-16345.
24. Vreeken, V.; Baij, L.; de Bruin, B.; Siegler, M. A.; van der Vlugt, J. I., N-Atom transfer via thermal or photolytic activation of a Co-azido complex with a PNP pincer ligand. *Dalton Trans.* **2017,** *46* (22), 7145-7149.
25. Zolnhofer, E. M.; Käß, M.; Khusniyarov, M. M.; Heinemann, F. W.; Maron, L.; van Gastel, M.; Bill, E.; Meyer, K., An Intermediate Cobalt(IV) Nitrido Complex and its N-Migratory Insertion Product. *J. Am. Chem. Soc.* **2014,** *136* (42), 15072-15078.
26. Sengupta, D.; Sandoval-Pauker, C.; Schueller, E.; Encerrado-Manriquez, A. M.; Metta-Magaña, A.; Lee, W.-Y.; Seshadri, R.; Pinter, B.; Fortier, S., Isolation of a Bimetallic Cobalt(III) Nitride and Examination of Its Hydrogen Atom Abstraction Chemistry and Reactivity toward H_2. *J. Am. Chem. Soc.* **2020,** *142* (18), 8233-8242.
27. MacLeod, K. C.; McWilliams, S. F.; Mercado, B. Q.; Holland, P. L., Stepwise N–H bond formation from N_2-derived iron nitride, imide and amide intermediates to ammonia. *Chem. Sci.* **2016,** *7* (9), 5736-5746.
28. Scepaniak, J. J.; Young, J. A.; Bontchev, R. P.; Smith, J. M., Formation of Ammonia from an Iron Nitrido Complex. *Angew. Chem. Int. Ed.* **2009,** *48* (17), 3158-3160.
29. Reactive Transition Metal Nitride Complexes. In *Progress in Inorganic Chemistry*, 2014; Vol. 58, pp 417-470.
30. Sun, Z.; Hull, O. A.; Cundari, T. R., Computational Study of Methane C–H Activation by Diiminopyridine Nitride/Nitridyl Complexes of 3d Transition Metals and Main-Group Elements. *Inorg. Chem.* **2018,** *57* (12), 6807-6815.
31. Ghannam, J.; Sun, Z.; Cundari, T. R.; Zeller, M.; Lugosan, A.; Stanek, C. M.; Lee, W.-T., Intramolecular C–H Functionalization Followed by a [2σ + 2π] Addition via an Intermediate Nickel–Nitridyl Complex. *Inorg. Chem.* **2019,** *58* (11), 7131-7135.
32. Man, W.-L.; Lam, W. W. Y.; Kwong, H.-K.; Yiu, S.-M.; Lau, T.-C., Ligand-Accelerated Activation of Strong C–H Bonds of Alkanes by a (Salen)ruthenium(VI)–Nitrido Complex. *Angew. Chem. Int. Ed.* **2012,** *51* (36), 9101-9104.
33. Thomson, R. K.; Cantat, T.; Scott, B. L.; Morris, D. E.; Batista, E. R.; Kiplinger, J. L., Uranium azide photolysis results in C–H bond activation and provides evidence for a terminal uranium nitride. *Nat. Chem.* **2010,** *2* (9), 723-729.
34. Long, A. K. M.; Timmer, G. H.; Pap, J. S.; Snyder, J. L.; Yu, R. P.; Berry, J. F., Aryl C–H Amination by Diruthenium Nitrides in the Solid State and in Solution at Room Temperature: Experimental and Computational Study of the Reaction Mechanism. *J. Am. Chem. Soc.* **2011,** *133* (33), 13138-13150.
35. Schlangen, M.; Neugebauer, J.; Reiher, M.; Schröder, D.; López, J. P.; Haryono, M.; Heinemann, F. W.; Grohmann, A.; Schwarz, H., Gas-Phase C–H and N–H Bond Activation by a High Valent Nitrido-Iron Dication and <NH>-Transfer to Activated Olefins. *J. Am. Chem. Soc.* **2008,** *130* (13), 4285-4294.
36. King, D. M.; Tuna, F.; McInnes, E. J. L.; McMaster, J.; Lewis, W.; Blake, A. J.; Liddle, S. T., Isolation and characterization of a uranium(VI)–nitride triple bond. *Nat. Chem.* **2013,** *5* (6), 482-488.
37. Mullane, K. C.; Ryu, H.; Cheisson, T.; Grant, L. N.; Park, J. Y.; Manor, B. C.; Carroll, P. J.; Baik, M.-H.; Mindiola, D. J.; Schelter, E. J., C–H Bond Addition across a Transient Uranium–Nitrido Moiety and Formation of a Parent Uranium Imido Complex. *J. Am. Chem. Soc.* **2018,** *140* (36), 11335-11340.
38. Scepaniak, J. J.; Margarit, C. G.; Harvey, J. N.; Smith, J. M., Nitrogen Atom Transfer from Iron(IV) Nitrido Complexes: A Dual-Nature Transition State for Atom Transfer. *Inorg. Chem.* **2011,** *50* (19), 9508-9517.
39. Schendzielorz, F. S.; Finger, M.; Volkmann, C.; Würtele, C.; Schneider, S., A Terminal Osmium(IV) Nitride: Ammonia Formation and Ambiphilic Reactivity. *Angew. Chem. Int. Ed.* **2016,** *55* (38), 11417-11420.
40. Yadav, M.; Metta-Magaña, A.; Fortier, S., Intra- and intermolecular interception of a photochemically generated terminal uranium nitride. *Chem. Sci.* **2020,** *11* (9), 2381-2387.
41. Park, S. V.; Fry, C. G.; Bill, E.; Berry, J. F., A metastable Ru^{III} azido complex with metallo-Staudinger reactivity. *Chem. Commun.* **2020,** *56* (73), 10738-10741.
42. Baek, Y.; Das, A.; Zheng, S.-L.; Reibenspies, J. H.; Powers, D. C.; Betley, T. A., C–H Amination Mediated by Cobalt Organoazide Adducts and the Corresponding Cobalt Nitrenoid Intermediates. *J. Am. Chem. Soc.* **2020,** *142* (25), 11232-11243.
43. Cenini, S.; Gallo, E.; Penoni, A.; Ragaini, F.; Tollari, S., Amination of benzylic C–H bonds by aryl azides catalysed by Co(porphyrin) complexes. A new reaction leading to secondary amines and imines. *Chem. Commun.* **2000,** (22), 2265-2266.
44. Ragaini, F.; Penoni, A.; Gallo, E.; Tollari, S.; Li Gotti, C.; Lapadula, M.; Mangioni, E.; Cenini, S., Amination of Benzylic C–H Bonds by Arylazides Catalyzed by Co^{II}–Porphyrin Complexes: A Synthetic and Mechanistic Study. *Chem. Eur. J.* **2003,** *9* (1), 249-259.
45. Fantauzzi, S.; Gallo, E.; Caselli, A.; Piangiolino, C.; Ragaini, F.; Cenini, S., The (Porphyrin)ruthenium-Catalyzed Aziridination of Olefins Using Aryl Azides as Nitrogen Sources. *Eur. J. Org. Chem.* **2007,** *2007* (36), 6053-6059.
46. Fantauzzi, S.; Gallo, E.; Caselli, A.; Ragaini, F.; Macchi, P.; Casati, N.; Cenini, S., Origin of the Deactivation in Styrene Aziridination by Aryl Azides, Catalyzed by Ruthenium Porphyrin Complexes. Structural Characterization of a Δ2-1,2,3-Triazoline RuII(TPP)CO Complex. *Organometallics* **2005,** *24* (20), 4710-4713.
47. Reaction coordinates involving direct phosphine reduction of the bridging azide were also investigated (see Supporting Information) but not found to exhibit lower energy profiles.
48. Saouma, C. T.; Peters, J. C., ME and ME complexes of iron and cobalt that emphasize three-fold symmetry (E=O, N, NR). *Coord. Chem. Rev.* **2011,** *255* (7), 920-937.
49. Gloaguen, Y.; Rebreyend, C.; Lutz, M.; Kumar, P.; Huber, M.; van der Vlugt, J. I.; Schneider, S.; de Bruin, B., An Isolated Nitridyl Radical-Bridged {Rh(N•)Rh} Complex. *Angew. Chem. Int. Ed.* **2014,** *53* (26), 6814-6818.
50. Angersbach-Bludau, F.; Schulz, C.; Schöffel, J.; Burger, P., Syntheses and electronic structures of μ-nitrido bridged pyridine, diimine iridium complexes. *Chem. Commun.* **2014,** *50* (63), 8735-8738.
51. Zhang, S.; Cui, P.; Liu, T.; Wang, Q.; Longo, T. J.; Thierer, L. M.; Manor, B. C.; Gau, M. R.; Carroll, P. J.; Papaefthymiou, G. C.; Tomson, N. C., N–H Bond Formation at a Diiron Bridging Nitride. *Angew. Chem. Int. Ed.* **2020,** *59* (35), 15215-15219.
52. The geometry optimized triplet state for ***lin*-^{2}$[Co_2N]^{3+}$** (∠Co–N–Co = 117°) was found to be nearly isoenergetic with the singlet (see Supporting Information).